Barapatre *et al. Bioresour. Bioprocess. (2016) 3:8*
DOI 10.1186/s40643-016-0083-y

Bioresources and Bioprocessing
a SpringerOpen Journal

RESEARCH Open Access

Synergistic antibacterial and antibiofilm activity of silver nanoparticles biosynthesized by lignin-degrading fungus

Anand Barapatre, Keshaw Ram Aadil and Harit Jha*

Abstract

Background: The fabrication of silver nanoparticles (Ag-NPs) through green chemistry is an emerging area in the field of medical nanotechnology. Ag-NPs were fabricated by enzymatic reduction of $AgNO_3$ using two lignin-degrading fungus *Aspergillus flavus* (AfAg-NPs) and *Emericella nidulans* (EnAg-NPs). The prepared Ag-NPs were characterized by different spectroscopic techniques. Antibacterial activity of prepared Ag-NPs was demonstrated against selected Gram negative (*Escherichia coli* and *Pseudomonas aeruginosa)* and Gram positive (*Staphylococcus aureus)* bacteria in the term of minimum bactericidal concentration (MBC) and susceptibility constant (Z). The synergistic antibacterial activity of Ag-NPs with four conventional antibiotics was also determined by the fractional inhibitory concentration index (FICI) using the checkerboard microdilution method. The antibiofilm potential of Ag-NPs was also tested.

Results: The plasmon surface resonance of biosynthesized Ag-NPs shows its characteristic peaks at UV and visible region (~450 and 280 nm). Fourier transform infrared spectrometer (FTIR) analysis confirms the nature of the capping agents as protein (enzyme) and indicates the role of protein (enzyme) in reduction of silver ions. The average particle size and charge of synthesized Ag-NPs was ~100 nm and ~−20 mV, respectively. X-ray diffraction (XRD) and TEM analysis confirmed the purity, shape, and size (quasi-spherical, hexagonal, and triangular) of Ag-NPs. Energy-dispersive X-ray spectroscopy (EDX) data validate the biological synthesis of Ag-NPs. Low MBC and high susceptibility constant indicate the high antimicrobial strength of biosynthesized Ag-NPs. The antibacterial analysis demonstrates the synergistic antimicrobial activity of Ag-NPs with antibiotics. This study also shows that biosynthesized Ag-NPs have ability to inhibit the biofilm formation by 80–90 %.

Conclusion: The *Aspergillus flavus* and *Emericella nidulans*-mediated biosynthesized Ag-NPs have significant antimicrobial activity and demonstrate synergistic effect in combination with antibiotics. It suggests that nanoparticles can be effectively used in combination with antibiotics to improve the efficacy of antibiotics against pathogenic microbes. The substantial antibiofilm efficiency of biosynthesized Ag-NPs would also be helpful against sensitive and multidrug-resistant strains.

Keywords: Silver nanoparticle, Synergistic antibacterial activity, Antibiofilm activity, *Aspergillus flavus*, *Emericella nidulans*

Background

Nanoparticles are currently an area of intense research due to a wide variety of potential applications in the biomedical, agricultural, optical, and electronic fields. Nanomedicine has now become one of the leading research thrust areas which involves synthesizing safe, biocompatible, effective, cheap, and non-toxic drugs to combat diseases (Durán et al. 2011; Keat et al. 2015). From the ancient time, silver is used globally, as an antimicrobial agent and currently used in various areas like biomedical sciences, drug delivery, diagnostics, personal care products, cosmetics, and other fields viz. imaging, optics, sensing, painting, due to unearthing many of

*Correspondence: harit74@yahoo.co.in
Department of Biotechnology, Guru Ghasidas Vishwavidyalaya (A Central University), Bilaspur, Chhattisgarh 495009, India

its properties in the nanometer-sized form. In the area of nanomedicine, its popularity is due to its high antimicrobial activity toward a broad range of pathogenic microbes and its relatively low toxicity toward humans (Sintubin et al. 2012; McShan et al. 2014; Khatami et al. 2015). It has been well documented and experimentally proven that silver nanoparticle has the highest antimicrobial property among known synthesized metal nanoparticles, with high level of biocompatibility. It was also observed that the effectiveness of antimicrobial property of nanoparticles depends on its size and increases with a decrease in size (Pal et al. 2007; Chudasama et al. 2010; Nath and Banerjee 2013).

The formation of metal nanoparticle by different physical and chemical, conventional approaches, requires several highly toxic chemicals which results in toxic side effects (Nath and Banerjee 2013). Green chemistry mediated synthesis of nanoparticle is, however, one of the alternative routes that not only reduces or eliminates the use of hazardous, toxic, and expensive chemicals, but also confirms the safety and efficacy with respect to process and product. Green synthesis also provides the cost effective, non-toxic, large-scale, and high-output nanoparticle products (Keat et al. 2015; Roy et al. 2013). Green chemistry mediated formation of nanoparticle is a kind of "bottom up" approach, where the main reaction is reduction/oxidation. In biologically mediated nanoparticle synthesis, the microbial enzymes or plant phytochemicals having reducing or antioxidant properties are usually responsible for the reduction of metal ions into their respective metal nanoparticles (Keat et al. 2015; Nath and Banerjee 2013; Chaturvedi and Verma 2015). Biosynthesis of silver nanoparticles using bacteria, fungi, and plants is already well documented (Durán et al. 2011; Chaturvedi and Verma 2015; Ingle et al. 2009; Thirunavoukkarasu et al. 2013). In fungal community, various fungal strains have been well reported, as an efficient bio-factory for the synthesis of metal nanoparticles (Ingle et al. 2009; Jaidev and Narasimha 2010; Saravanan and Nanda 2010).

Several reports have successfully demonstrated that Ag-NPs have antimicrobial activity against a broad range of gram-negative and gram-positive pathogenic bacteria including *Escherichia coli, Pseudomonas aeruginosa*, and *Staphylococcus aureus* (Keat et al. 2015; Pal et al. 2007; Ingle et al. 2009; Jung et al. 2008; Li et al. 2011). The mechanism of the antimicrobial action of silver nanoparticle was proposed by different authors, in which the most common were the disruption in ATP production, error prone DNA replication, generation of reactive oxygen species, failure of the proton motive force system, and direct damage to cell membranes (Marambio-Jones and Hoek 2010). Crystallographic surface structure and high surface-to-volume ratio amplify the contact area of metallic nanoparticles with a microorganism-influencing antibacterial activity of nanosized silver particle (Kora and Arunachalam 2011).

In the present study, Ag-NPs were biosynthesized extracellular using two fungi from Ascomycota member, *Aspergillus flavus* and *Emericella nidulans*. Biosynthesized Ag-NPs were extensively characterized by different spectrophotometric methods, and their synergistic antimicrobial activity with different classical antibiotics was evaluated against three common opportunistic pathogenic bacteria by the checkerboard microdilution method. The antibiofilm potential of biosynthesized Ag-NPs was also determined.

Methods

Reagents

All reagents were analytical grade and purchased from Merck Inc. (Mumbai, India). Antibiotics [Amikacin (AMI), Kanamycin (KAN), Oxytetracycline (OXY), Streptomycin (STR)] used in the experiments were purchased from Sigma and Hi-Media (Mumbai, India). Ultrapure Milli-Q water (Elix, Merck Millipore, Mumbai, India) was used to prepare the antibiotic and Ag-NPs dilutions.

Source of microorganisms

Two fungal strains *A. flavus* (F10, NCBI accession no. KC911631.1) and *E. nidulans* (APF4, NCBI accession no. KC911632.1) reported for lignin degradation were used for the preparation of Ag-NPs. Three bacterial strains namely, *E. coli* (gram-negative rods, MTCC-739), *P. aeruginosa* (gram-negative cocci, MTCC-741), and *S. aureus* (gram-positive cocci, MTCC-96) were procured from the microbial-type culture collection (MTCC), IMTECH, Chandigarh, India and used in the investigation of antimicrobial properties of Ag-NPs. All three bacterial cultures were grown overnight on Luria–Bertani agar (LB) slants and maintained at 4 °C for further experiments.

Green synthesis of Ag-NPs

Production of biomass

For the production of biomass, the fungus was grown aerobically in the liquid broth production medium. For *A. flavus*, Czapek Dox yeast broth (sucrose 30 g/L, yeast extract 5 g/L, $MgSO_4.7H_2O$ 0.5 g/L, $NaNO_3$ 2 g/L, KCl 0.5 g/L, $FeSO_4.7H_2O$ 0.001 g/L; pH-5.8) and for *E. nidulans*, Czapek Dox broth (sucrose 30 g/L, $NaNO_3$ 2 g/L, K_2HPO_4 1 g/L, $MgSO_4.7H_2O$ 0.5 g/L, KCl 0.5 g/L, $FeSO_4.7H_2O$ 0.001 g/L; pH-5.8) were used, respectively. The culture flasks were incubated in static condition at 37 and 27 °C, respectively. The fungal mat was separated from 5 days old production medium by filtration through

Whatman filter paper no. 4 and washed three times with sterile double-distilled water to remove the media components from the biomass.

Synthesis of Ag-NPs

Typically 10 g of biomass (wet weight) of both fungi was incubated in 100 mL sterilized Milli-Q water for 3 days at 27 °C in shaking condition on an orbital shaker at 100 rpm. After the incubation, fungal suspension was separated by filtration through Whatman filter paper no. 1 and the resulting filtrate was divided in two equal parts. In the first part of the filtrate, (50 mL) $AgNO_3$ was added so that the final concentration of $AgNO_3$ reached 1 mM, and the other half of filtrate (50 mL) devoid of $AgNO_3$, served as a control. Both flasks were kept on orbital shaker at 27 °C in 100 rpm under dark conditions.

Characterization of Ag-NPs

UV–visible spectrophotometry

The reduction of Ag^+ ions and formation of Ag-NPs was monitored every 24 h by taking the UV-visible spectra of the reaction medium. After diluting an aliquot of 1 mL of the reaction medium with 2 mL Milli-Q water, spectra was measured in the range of 250–700 nm using a UV-1800 spectrophotometer (Shimadzu, Japan).

Fourier transform infrared spectroscopy (FTIR)

FTIR measurements were performed to investigate the associated molecules with Ag-NPs. The Ag-NPs solution (100 mL) was centrifuged at 20,000 rpm for 10 min. The samples were dried and ground with potassium bromide (KBr) pellets (1:100 w/w) and analyzed by Affinity-1 model (Shimadzu, Japan) at a spectral range 4000–400 cm^{-1} at a resolution of 4 cm^{-1}. The FTIR analysis of cell-free extracts was also performed which serves as a reference.

Dynamic light scattering (DLS)

The particle size distribution and Zeta (ζ) potential measurements of Ag-NPs were performed with a Zeta Sizer (Malvern Zeta Sizer Nano ZS90, UK) at room temperature. The sample preparation for zeta analysis involves the mixing of biosynthesized Ag-NPs in Millipore water in 1:10 (v/v) proportion, total volume of the sample was 2 mL, taken in the clean zeta cell for the measurement of Zeta potential.

X-ray diffraction (XRD)

XRD analysis was carried out using an X-ray powder diffractometer (PANalytical 3 kW X'Pert Powder). The air dried nanoparticles were coated onto XRD grid and analyzed at a voltage of 40 kV and a current of 30 mA with Cu K_α monochromatic radiation ($k = 0.15406$) (Fazay et al. 2011). The diffracted intensities were recorded from 25 to 85 of 2θ angles with a step of 0.02° at room temperature (27 °C).

Transmission electron microscopy (TEM)

TEM analysis was undertaken to know the size and shape of the Ag-NPs biosynthesized using fungus. After synthesis of Ag-NPs, the sample was washed several times with sterilized Milli-Q water. TECNAI 20 G2 200 kV TEM (Fei, Electron Optics, Netherland) was employed to get the TAM images of Ag-NPs. A drop of the Ag-NPs solution was loaded on the carbon-coated copper grid and allowed to dry. A voltage of 200 kV and magnification at 15,000× and 19,500× were used for observing the nanoparticles. The particle size of Ag-NPs was also determined through the image processing software ImageJ (Version 1.49, NIH, USA). The polydispersity of synthesized Ag-NPs, based on TEM image data, was calculated according to Zhao et al. (2015).

Energy-dispersive X-ray spectroscopy (EDX)

EDX analysis was conducted using Phillips CM20-Ultra Twin microscope operating at 200 kV, to confirm the elemental composition, associated with the Ag-NPs.

Analysis of antibacterial activity of biosynthesized Ag-NPs

Determination of minimum bactericidal concentration (MBC) and susceptibility constant

The MBC of each Ag-NPs was determined by colony forming unit (CFU) assay as per following protocol. Test bacteria were grown in fresh LB medium at 37 °C in a gyratory shaker (Remi, India) at 135 rpm to obtain an optical density (OD) of 0.05 (correspond to ~10^8 cells/mL) at 600 nm. In 10 mL of the above medium, different concentrations of Ag-NPs ranging from 1 to 64 µg/mL were added, and the culture tubes were allowed to incubate at 37 °C in a gyratory shaker at 135 rpm for 18–20 h. Control cultures without nanoparticles were included in experiments, and the number of CFU (i.e., the number of bacteria present) recovered after the 18 h incubation was enumerated. From the above incubated cultures, a fixed amount of media was withdrawnserially diluted in saline (0.85 % NaCl, w/v). Properly diluted samples (100 µL) were spread on LB agar plates and incubated at 37 °C for 18–24 h, until the colonies appeared and the numbers of CFU were counted manually. Final CFU was determined by multiplying the dilution factor with the viable number of colonies. The culture that showed the decrease of 99.9 % in CFU after incubation was determined as MBC (Chatterjee et al. 2012).

Susceptibility constant of different bacteria against Ag-NPs was determined according to Chatterjee et al. (Chatterjee et al. 2012). A higher *Z value* means a higher

sensitivity of bacteria toward the nanoparticles, and the nanoparticles have more effective antimicrobial activity. The susceptibility constant (Z) of a bacterial population to an antimicrobial compound is calculated as $Z = -\text{In}\ (N/N_0)/C$, where N_0 and N are the numbers of living cells at 0 h and after 16–20 h incubation at the substance concentration C. Therefore, at MBC, $Z = 3\text{In}10/\text{MBC} = 6.908/\text{MBC}$ (Chatterjee et al. 2012).

Evaluation of synergistic effects between Ag-NPs and antibiotics by broth microdilution checkerboard method

The degree of synergy between antibacterial drugs is often expressed in terms of the fractional inhibitory concentration (FIC). The FIC is the minimum inhibitory concentration (MIC) of the drug in combination divided by the MIC of drugs acting alone. Four antibiotics drugs, namely amikacin (AMI), kanamycin (KAN), oxytetracycline (OXY), and streptomycin (STR) were used to examine their combined synergistic effects with prepared Ag-NPs against the selected pathogenic bacterial species. Stock solutions of these agents were prepared in sterile Millipore water to a concentration from 1 to 128 µg/mL and refrigerated at 2–4 °C. A checkerboard microdilution technique was used to examine the synergism between the antibiotics and Ag-NPs against test organisms.

For the determination of the factional inhibitory concentration (FIC), the microdilution "checkerboard" method was applied in microwell-containing plates. In this method, minimum inhibitory concentration (MIC) was determined, for both antibiotics and Ag-NPs alone and in their paired combinations (Isenberg 2007). For antibiotics and Ag-NPs, the test range was 0.5–128 µg/mL. The sterility of prepared microwell plates was checked by incubation it in 37 °C for 24 h. Bacterial inoculum was prepared from an 18–24 h incubation of the test organism grown on Muller-Hinton broth (MHB). The organisms were harvested, and suspended in sterile MHB to produce a McFarland, 0.5 (turbidity equivalent to 10^8 colony forming units). The 0.5 McFarlands suspension was diluted in fresh MHB to achieve final CFU of 4×10^6 to 5×10^6 from which 0.01 mL was inoculated into the microwells. The bacterial inoculated microtitre plates were incubated at 37 °C for 16–20 h.

The lowest concentration at which no visible growth occurred was recorded to be the MIC value of the individual and combined test agents. FIC was calculated from the MIC of the test agent A and the MIC of the test agent A in combination with test agent B. Therefore,

$$\text{FIC of antibacterial A} = \text{MIC of antibacterial A in combination}/\text{MIC of antibacterial A alone}$$

The FIC of antibacterial agent B was calculated in the same manner and the sum of the two FIC agents combined to give the ΣFIC index.

$$\Sigma\text{FIC index} = \text{FIC of antibacterial A} + \text{FIC of antibacterial B}$$

The calculated FIC index was used to detect the nature of interaction between the two test agents and the interaction either synergism or indifference or antagonism type. The values published by the American Society of Microbiology were used to decide the nature of the interaction FICI < 0.5 synergy, $0.5 \leq \text{FICI} < 1$ partial synergy, FICI = 1 additive, $2 \leq \text{FICI} < 4$ indifferent, and 4 < FICI antagonism (Botelho 2000).

Antibiofilm potential of Ag-NPs

To determine the efficacy of Ag-NPs in biofilm formation, 96-well microtiter plate method was applied (Kalishwaralal et al. 2010). Individual wells of the sterile microtiter plate were filled with 180 µL of MH broth and inoculated with 10 µL of overnight grown culture. To the mixture, 10 µL of silver nanoparticles was added from the stock so that the final concentration of nanoparticle was achieved between 0.5 and 64 µg/mL. The microtiter plates were incubated for 24 h at 37 °C. After incubation, content of each well was gently removed and washed with 0.2 mL of phosphate buffer saline (PBS, pH 7.2) three times, to remove free-floating 'planktonic' bacteria. Biofilms formed by adherent 'sessile' organisms in plate wall were fixed with sodium acetate (2 %, w/v) and stained with crystal violet dye (0.1 %, w/v). Excess stain was rinsed off by thorough washing with sterilized Millipore water and plates were kept for drying. After drying, 200 µL of 95 % (v/v) ethanol was added to the wells. The absorbance at 620 nm was measured on an ELISA reader (Multiskan® EX, Thermo Scientific, Finland), and values obtained were considered as an index of bacteria adhering to the surface of well wall for developing biofilms. The percentage of biofilm inhibition was calculated using the equation:

$$\%\ \text{biofilm inhibition} = \left[1 - \left(\text{OD}_{620}\text{of cells treated with Ag} - \text{NPs}/\text{OD}_{620}\text{of non-treated control}\right) \times 100\right].$$

Experiment was performed in triplicate, the data were then averaged, and the standard deviation was calculated. The fungal cell-free filtrate (10 µL), used for the Ag-NPs preparation, serves as a positive control.

Results and discussion

UV–visible spectroscopy

UV–visible spectroscopy is one of the simplest and most used technique for the preliminary characterization of silver

nanoparticle. The optical signature of metal nanoparticles is given by the surface plasma resonance (SPR) and it is crucial to understand the number, position, and width of the SPRs as a function of the NP shape, size, and environment. SPR is affected by properties like surface charge distributions, dielectric medium, and surface-absorbed species, which are directly associated with nanoparticle size (Noguez 2007).

UV–visible spectra of fungal culture filtrate containing silver nanoparticles were obtained at regular time interval and presented in Figs. 1a, 2a. The extracellular synthesis of Ag-NPs was observed during incubation of culture filtrate of fungus and silver nitrate salts. A gradual change observed in coloration from light yellow to dark brown is an indication of the formation of Ag-NPs. From the spectral study, it was observed that *E. nidulans* synthesized Ag-NPs (EnAg-NPs) show the surface plasmon resonance band maxima of silver nanoparticles centered at 450 nm, whereas *A. flavus* synthesized Ag-NPs (AfAg-NPs) show the broad peak range from 420 to 450 nm. The intensity of peaks steadily increases with incubation time. Ag-NPs formed from both organism display a red shift in wavelengths from its characteristic resonance peak for spherical silver nanoparticle at 420 nm. Noguez (Noguez 2007) explained that the small particle size metal nanoparticles (<40 nm) surface resonances do not change their characteristic position or frequency, but they become wider because of surface dispersion effects. However, with the increase in particles size and transformation in the nanoparticle morphology (i.e., spherical to the icosahedral/cuboctahedron/truncated cube), the optical absorption spectra of metal nanoparticles, dominated by surface plasmon resonances (SPR), shift toward longer wavelengths and also make the peaks broader. A broadening in the absorption peak of AfAg-NPs can be also explained by Mie's theory. Mie's theory explains that the number of SRP bands of the nanoparticle is dependent on its shape. Spherical nanoparticle produces single SRP band while the anisotropic particle produces more SRP bands in optical absorption spectra (Pal et al. 2007). A small shoulder also appears in the absorption spectrum of EnAg-NPs at ~360 nm, which may be due to smaller colloids, absorbing at shorter wavelengths.

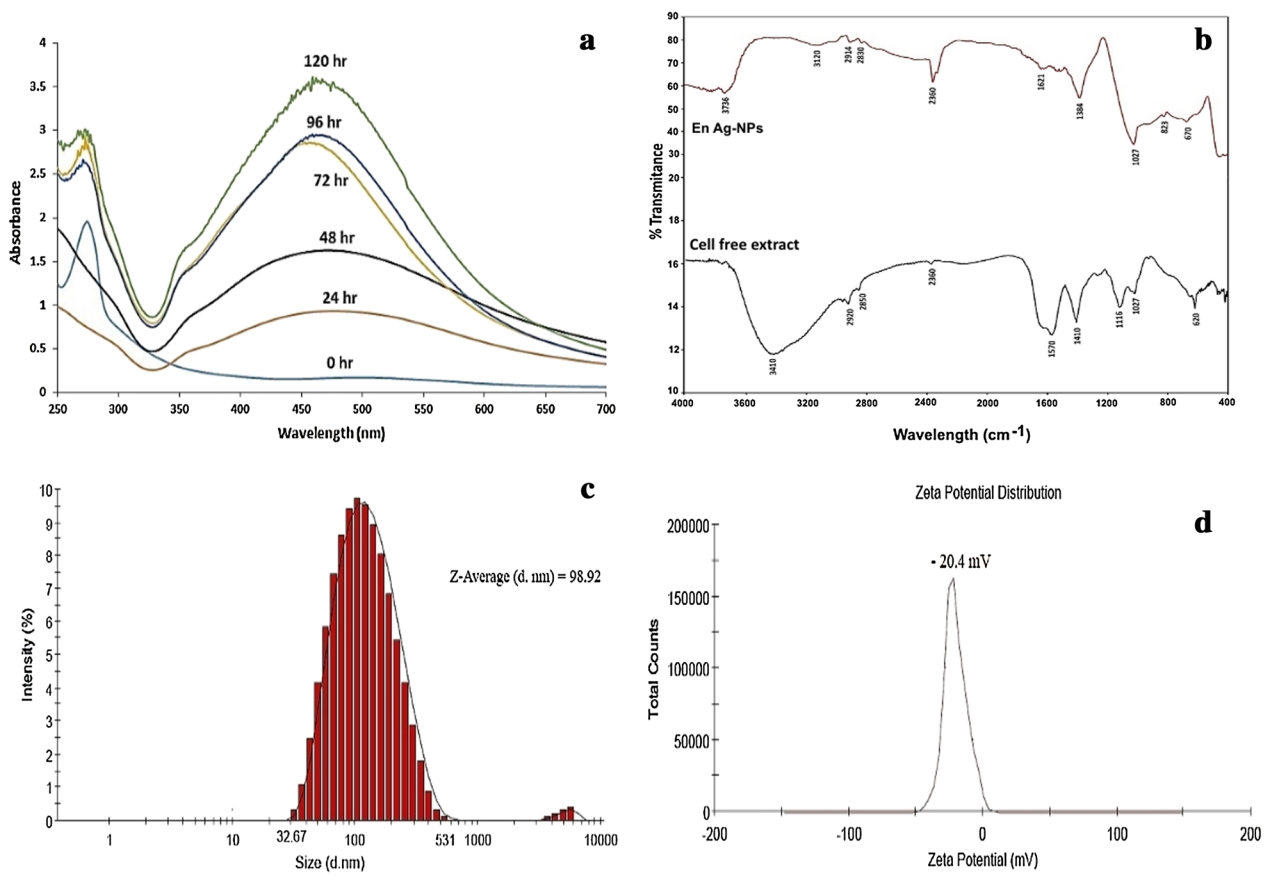

Fig. 1 Characterization of *E. nidulans* synthesized silver nanoparticles **a** UV–visible spectra, **b** FTIR spectrum, **c** histogram of particle size distribution, **d** zeta potential

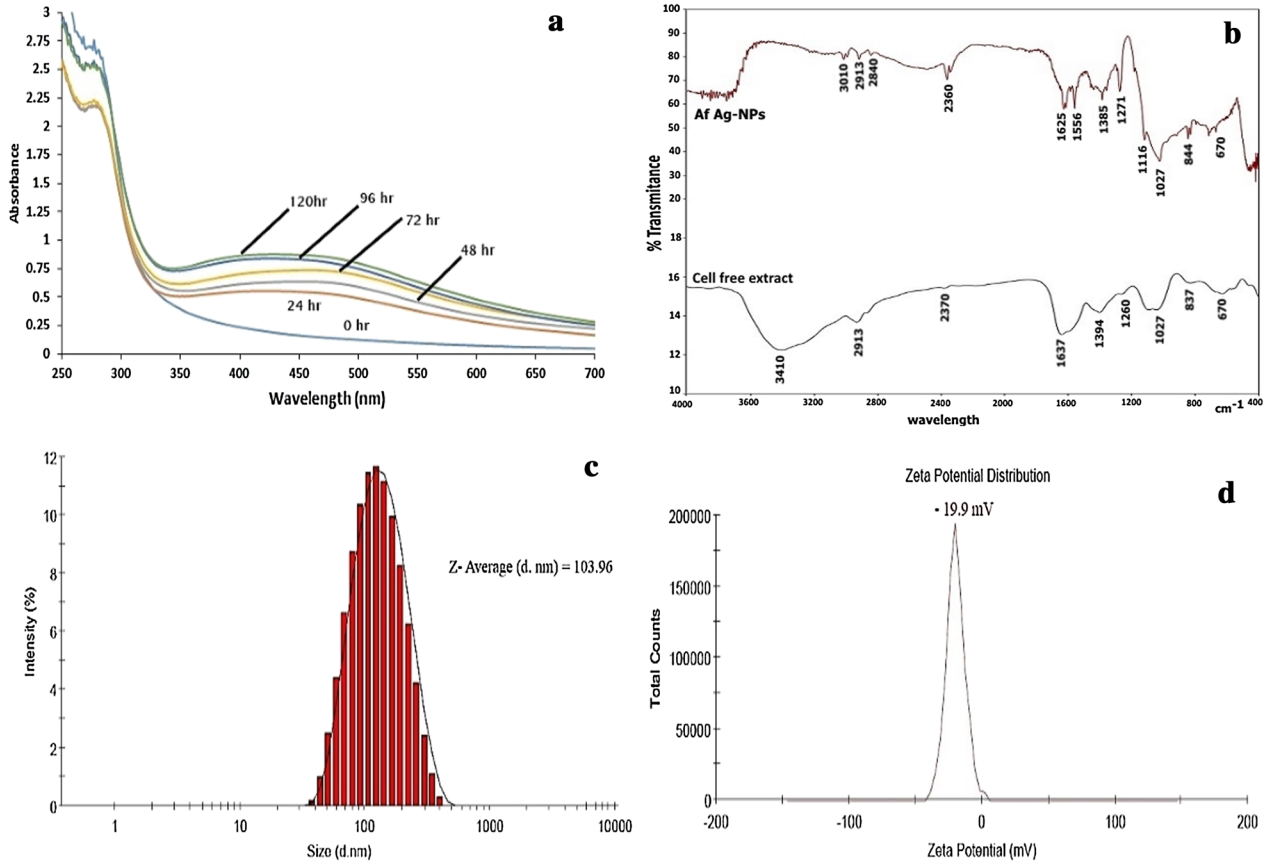

Fig. 2 Characterization of *A. flavus* synthesized silver nanoparticles **a** UV–visible spectra, **b** FTIR spectrum, **c** histogram of particle size distribution, **d** zeta potential

Both EnAg-NPs and AfAg-NPs spectra produce an absorption peak in UV region at 280 nm. This peak may be due to the electronic extinction of aromatic amino acid (tryptophan and tyrosine) in protein residue (Vigneshwaran et al. 2007; Fayaz et al. 2010). This observation suggests the involvement of extracellular proteins of fungus in the formation and stability of the nanoparticles.

FTIR analysis

The FTIR analysis was performed to identify the functional group of the attached capping biomolecule, responsible for the reduction, synthesis, or stabilization of the nanoparticles. The FTIR spectra (Figs. 1b, 2b) of both Ag-NPs display bands at 1388 and 1385 cm^{-1} which is assigned for functional group of residual NO^{3-} (Ramaswamy et al. 2012). EnAg-NPs display bands at 2914 and 1534 cm^{-1} which were assigned to the main and the corresponding stretching vibration of –N–H in secondary amine (amide II) while 1647 cm^{-1} was assigned for –C=O stretch vibration in primary amine (amide I). Band observed at 1510 and 1030 cm^{-1} can be allotted to the amide II functional group and C–N stretching vibration of aliphatic amine, respectively. FTIR spectrum of AfAg-NP displays bands corresponding to stretching vibration of –N–H in secondary amine (amide II) at 2913 and 1556 cm^{-1}, whereas band at 1621 cm^{-1} correspond to –C=O of the primary amine (amide I). Band at 1273 cm^{-1} is corresponding to strong stretching vibrations of C–N aromatic and aliphatic amines. All the above peaks present in Ag-NPs IR spectrum, are also present in the IR spectrum of the cell-free filtrate of both fungi (Figs. 1b, 2b). The absorbance of all corresponding peaks was high in cell-free filtrate as compared to the Ag-NPs. The presence of all above signature peaks of amino acids in the IR spectrum, confirms the presence of proteins/enzymes in the cell-free filtrate as well as in both Ag-NPs (Fazay et al. 2011; Jain et al. 2011). Peak at 1027 cm^{-1}, suggested the involvement of phosphate bonds in the reduction of silver ion (Durán et al. 2011). Ingle et al. (2009) and Ramaswamy et al. (2012) also reported that the biological synthesis of Ag-NPs is mediated through the proteins (enzymes) like NADH-dependent nitrate reductase of source microorganism. In protein, carbonyl group, amine groups, cysteine residues, and peptides have stronger

ability to bind and stabilize silver ions through the electrostatic attraction (Durán et al. 2011; Jain et al. 2011).

Particle size distribution and zeta potential

The particle size and the zeta potential of the prepared nanoparticle are the main factors that interfere with the biological activities and its reaction with other active charge surface. The antimicrobial mechanism of nanoparticles varies, depending on their variation in particle size and zeta potential (Bihari et al. 2008).

From Figs. 1c, 2c it is evident that the Ag-NPs formed by fungus have a wide range of size. The EnAg-NP displays a range from 36 to 531 nm while AfAg-NPs were in the range of 37–340 nm. The z-average values for EnAg-NPs and AfAg-NPs were 98.92 and 103.96, respectively, whereas the polydispersity index (PDI) was low i.e., 0.272 and 0.224, respectively. The surface zeta potential values of Ag-NPs (Figs. 1d, 2d) were measured to be slightly negative and were −20.4 mV for EnAg-NPs and −19.9 mV for AfAg-NPs. The negative charge of Ag-NPs prevents them from aggregation and increases their stability, as well as help enhance their antimicrobial property. The possible cause of the negative surface charges on synthesized Ag-NPs is the absorption of free nitrate ions present during the reduction of $AgNO_3$ (Kim et al. 2007).

X-ray diffraction analysis

The XRD patterns of the prepared Ag-NPs from *E. nidulans* and *A. flavus* are shown in Figs. 3a, 4a. The Fig. 3a, shows diffraction peaks for EnAg-NPs, (2θ) at 38.2°, 44.4°, 64.6°, 77.5°, and 81.7°, which can be indexed to the (111), (200), (220), (311), and (222) planes of the face-centered cubic (fcc) silver (Joint Committee on Powder Diffraction Standards file no. 04-0783). It confirmed silver as the main component of the nanoparticle. The predominant orientation was the (111) plane because the most intense peak appeared at 38.2°. The diffractogram did not suggest the presence of possible impurities such as $AgNO_3$ or Ag_2O (Fazay et al. 2011), whereas AfAg-NP diffractogram (Fig. 4a) shows the diffractions at 38.3°, 44.4°, 64.6°, 77.47°, and 81.6° that can be indexed to the (111), (200), (220), (311), and (222) planes of the fcc. In the AfAg-NPs diffractogram, some other peaks at 28°, 32.3°, 46.3°, 54°, and 57.8° were also produced. The formation of these peaks in XRD diffractogram might be due to the presence of associated contaminations with biosynthesized Ag-NPs. Yoon et al. (2007) also found the peaks at 28° and 32.3° in XRD diffractogram of fungus-mediated Ag-NPs and suggested that the origin of these peaks might be due to the interaction of silver with the fungal cell wall.

EDX

The elemental analysis of the Ag-NPs was performed using the EDX. The EDX spectrum of the biosynthesized Ag-NPs is shown in Figs. 3b, 4b, which reveals the existence of various elements. In both EDX spectra of Ag-NPs, peaks around 3 keV correspond to the binding energies of Ag_L (Jain et al. 2011), while the peaks of N_k, C_k, O_k, and K_k were situated near the 0.5 keV. In spectra, the weight % of Ag was 34.01 and 41.42, for EnAg-NPs and AfAg-NPs, respectively. Also, a peak near 1.1 keV corresponding to Na_k and Mg_k, was observed. Beside Ag, there are other elemental peaks bands for S, Mg, N, C, O, and P that also appeared throughout the scanning range (0–4 keV) of the spectrum suggesting that the biological origin molecule i.e., enzymes or proteins were attached with the biosynthesized Ag-NPs, further the presence of protein or enzyme like molecule was also confirmed by the UV–visible and FTIR spectroscopy (Durán et al. 2011; Jain et al. 2011; Li et al. 2012). From the EDX results it was also proposed that the synthesized Ag-NPs might be stabilized through these proteins or enzyme. Li et al. (2012) also studied the Ag-NPs preparation through *A. terreus* supernatant and confirmed that the NADP-dependent reductase was involved in the formation of Ag-NPs. The overall results indicate that the synthesized Ag-NPs were formed by the enzymatic reduction.

Transmission electron microscopic analysis

Morphology of the synthesized Ag-NPs was characterized by TEM study. Figures 3c, 4c show the TEM image for *E. nidulans* and *A. flavus*, respectively, captured from the nanoparticle-coated carbon grid. The EnAg-NPs display a high uniformity in comparison to AfAg-NPs. As evident in Fig. 3c morphology of EnAg-NPs were mono dispersive and mostly having hexagonally shaped nanoparticle, while *A. flavus* (Fig. 4c) formed mostly quasi-spherical Ag-NPs, few were triangular and hexagonal in shape. The particle size of both Ag-NPs ranges from 30 to 150 nm as deduced by TEM micrograph. The particle size histogram (EnAg-NPs and AfAg-NPs) based on the TEM image (Figs. 3d, 4d) shows that the most of Ag-NPs come under the ranges of 10–450 nm, and in both frequency distribution histogram of Ag-NPs the major portion of particles (80–90 %) fall in the range of 5–100 nm. Based on the TEM image analysis by ImageJ software, it was determined that EnAg-NPs and AfAg-NPs possess an average particle size of 66.68 and 81.11 nm, respectively. These results are in agreement with the values obtained by DLS measurements. The polydispersity indices of EnAg-NPs and AfAg-NPs are 48.83 and 18.68, respectively, as determined by the ImageJ software Ag-NPs size calculation.

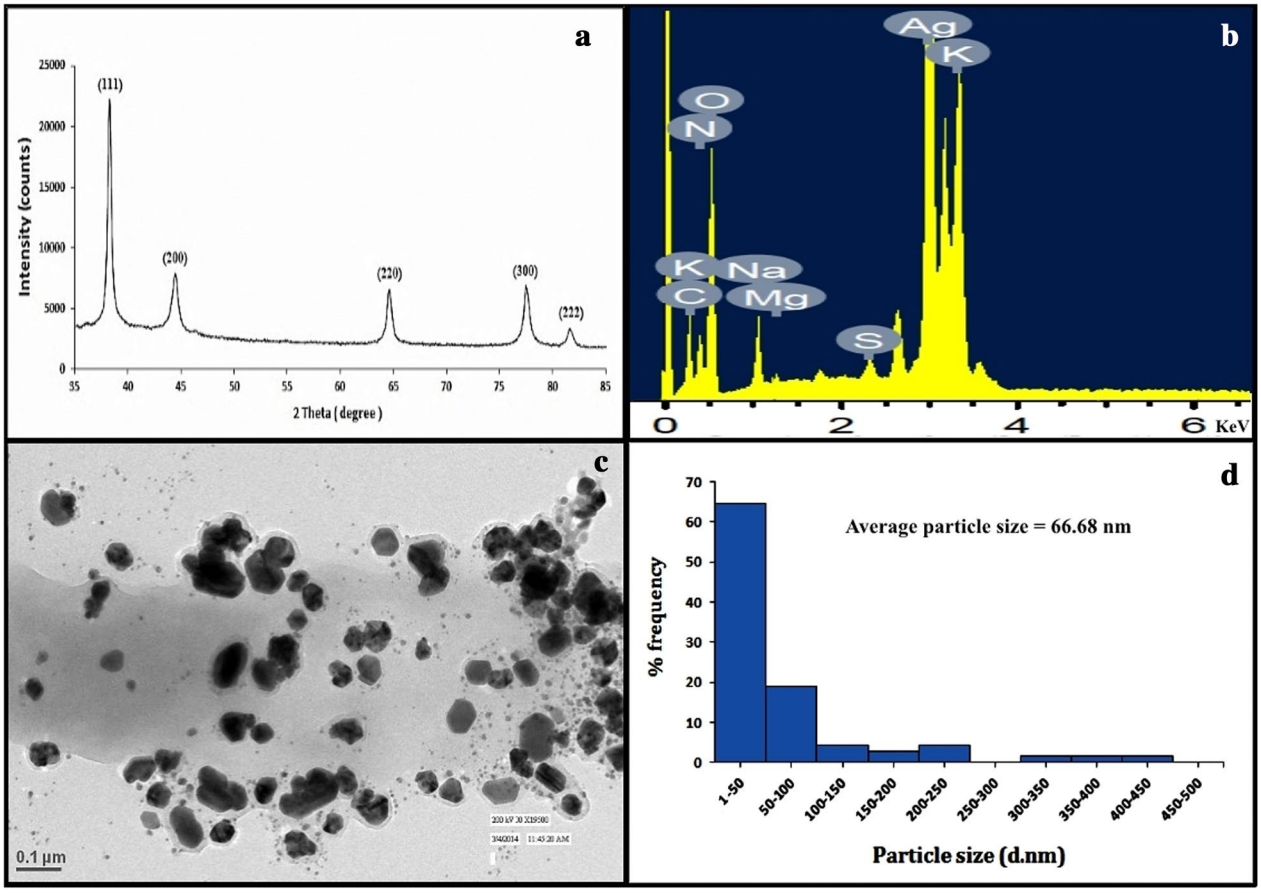

Fig. 3 Characterization of *E. nidulans* synthesized silver nanoparticles **a** XRD diffractogram , **b** EDX spectrum, **c** TEM image, and **d** Particle size distribution histogram (based on TEM image)

It was seen that through the enzymatic synthesis process, the formation of quasi-spherical NPs was most common, but the morphology of NP depends on the metal ion solution, concentration of biomolecule produced by the microbes, incubation time, and incubation condition (Quester et al. 2013). Several other members from same fungal family were also reported for the Ag-NPs formation viz. *A. fumigatus* [mostly spherical some triangular, 5–25 nm; (Bhainsa and D'Souza 2006)], *A. flavus* [spherical; 17 nm, (Jain et al. 2011)], *A. clavitus* [550–650 nm; (Saravanan and Nanda 2010)], *A. terreus* [spherical, 1–20 nm; (Li et al. 2012)] *A. niger* [spherical, 3–30 nm; (Jaidev and Narasimha 2010)], *A. temerii* [spherical, 25–50 nm; (Ramaswamy et al. 2012)]. The literature thus suggests that most of the fungi of this family synthesize spherical-shaped Ag-NPs till date, and to the best of our knowledge, this is the first report in contrast to the extracellular synthesis of Ag-NPs by *E. nidulans* and as well as the hexagonal- and triangular-shaped Ag-NPs formed by both of this fungus.

MBC and Susceptibility constant

To investigate the antibacterial potential (MBC) of the silver nanoparticle against *E. coli, S. aureus*, and *P. aeruginosa*, a broth dilution method and the conventional plate count technique (CFU counting) were carried out in LB medium. All test bacterial strains (approximately 10^8 cells/mL) were grown overnight in the presence of different concentrations of Ag-NPs (1–64 µg/mL). After 18–24 h incubation, the viability of the bacterial cells was determined by CFU counting. The MBC values of both Ag-NPs are presented in Table 1. The results show that the efficacy of AfAg-NPs was higher than EnAg-NPs, against *E. coli* with lower MBC. In case of *P. aeruginosa*, AfAg-NPs was found more potently bactericidal than EnAg-NPs, while against *S. aureus*, EnAg-NPs was more effectively bactericidal than AfAg-NPs.

Pelletier et al. (2010) suggested that the reactivity of nanoparticle against microbes is highly dependent on the morphology as well as surface-to-mass ratio. Smaller, uneven, and irregular-shaped particle has different binding characteristic with the microbial surface,

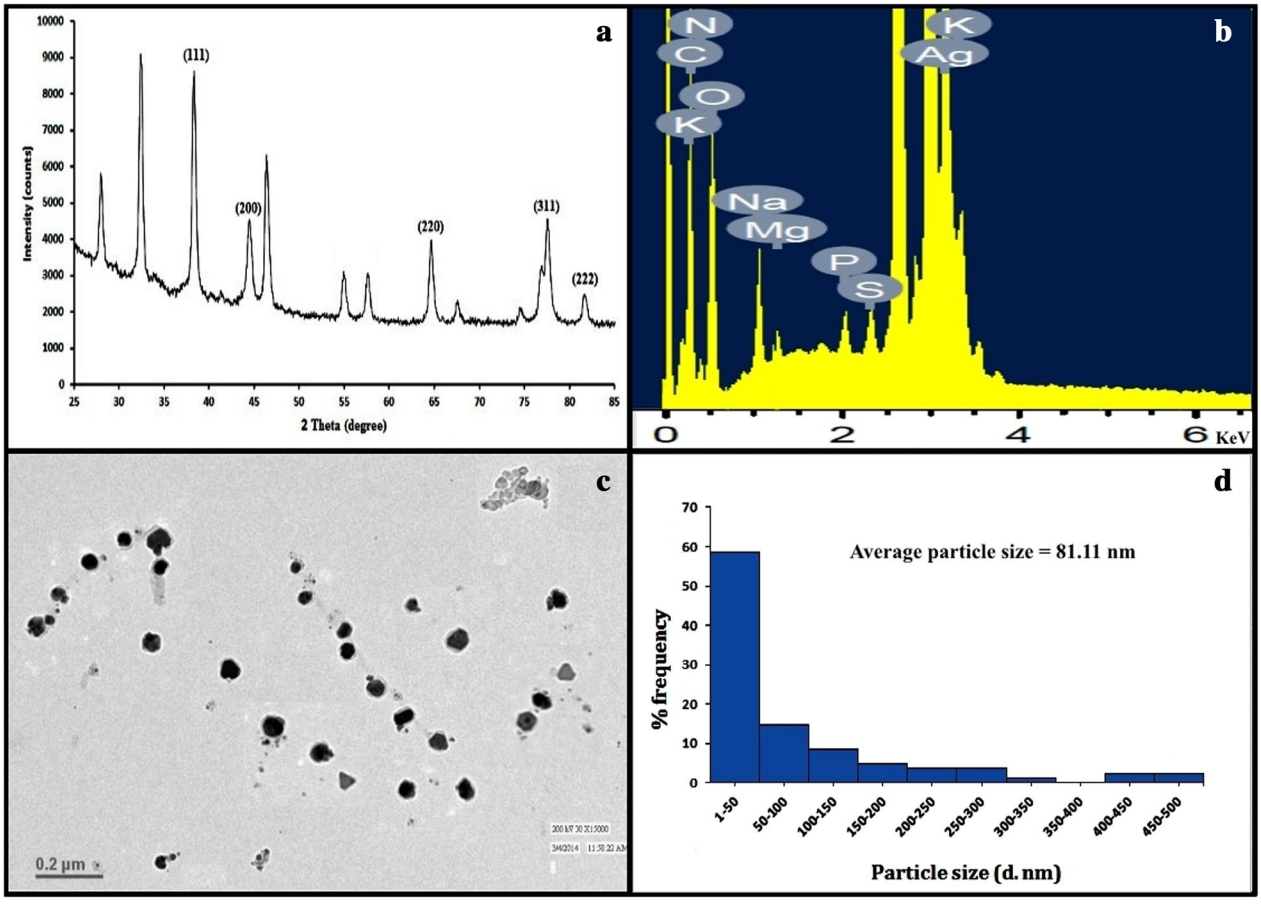

Fig. 4 Characterization of *A. flavus* synthesized silver nanoparticles **a** XRD diffractrogram, **b** EDX spectrum, **c** TEM image, and **d** particle size distribution histogram (based on TEM image)

due to itsbiological and chemical reactive edges and corners. The Ag-NPs prepared from both fungi have a wide range of particle size distribution. Results show an effective bactericidal activity against test organisms. Pal et al. (2007) explained the shape-dependent antimicrobial activity of nanoparticles in the term of active facets. They found that the high atom density facets, such as {111} facets have high antimicrobial activity. The result in the present study is in strong agreement with the XRD result of nanoparticle. Both nanoparticles show a prominent peak of {111} facets. The XRD pattern correlated with TEM analysis that there are lots of differently shaped viz. hexagonal-, triangular-, and quasi-spherical-shaped nanoparticles present in the sample, and contain high {111} facets, which increase their antibacterial activity.

Along with the MBC, the susceptibility constant (Z) is also an important factor in the antimicrobial study of silver nanoparticles, which is a quantitative parameter for antimicrobial power toward specific bacteria (Yoon et al. 2007). In the present study, the *Z values* of *E. coli*, *P. aeruginosa,* and *S. aureus* of EnAg-NPs are 0.216, 0.216, and 0.288 mL/µg, respectively, while in the case of AfAg-NPs, it is 0.288, 0.216, and 0.288 mL/µg. These results depict that *S. aureus* is most sensitive, whereas *P. aeruginosa* was most resistant toward both Ag-NPs. While *E. coli* was more sensitive toward AfAg-NPs than EnAg-NPs. The difference in the activity of Ag-NPs was possibly due to the difference in the membrane structure of Gram-negative and Gram-positive bacteria. Physical interaction of Ag-NPs with the bacterial

Table 1 Minimum bactericidal concentration (MBC; in µg/mL) of the both Ag-NPs

Test organism	Ag-NPs synthesized by	
	E. nidulans	***A. flavus***
S. aureus	24 > MBC > 16	MBC ≤ 24
E. coli	32 > MBC > 24	24 > MBC > 16
P. aeruginosa	64 > MBC > 32	32 > MBC > 24

cell may lead to increased membrane permeability and cause physical damage, which ultimately leads to cell death.

Synergistic effect of Ag-NPs with different antibiotics

The synergistic effects of Ag-NPs were also investigated with four conventional antibiotics against pathogenic bacteria using checkerboard microdilution method and the effects were evaluated by determination of the FICI. The results of the synergistic effect in the form of ΣFIC range and mean FIC are presented in Tables 2, 3, respectively. All of the combinations demonstrated synergistic and partial synergistic effect against the tested bacteria. An enhanced antibacterial synergistic activity of EnAg-NPs and three antibiotics (KAN, OXY, and STR) was found against *S. aureus*, whereas AfAg-NPs with all antibiotics show partial synergism. The AfAg-NPs display more antibacterial activity than EnAg-NPs against *S. aureus*. In the case of *E. coli*, both Ag-NPs show synergistic activity with AMI and STR, while other two display partial synergism. A partial synergistic interaction of AfAg-NPs was observed with all four antibiotics against *P. aeruginosa*, whereas EnAg-NPs produce partial synergistic with AMI and STR. The other combinational activities (EnAg-NPs with KAN and OXY) were found as antagonistic activity against *P. aeruginosa*. These synergistic activities of Ag-NPs in the presence of conventional antibiotics suggest that it might be possible to reduce the viability of bacterial strains at lower antibiotic concentrations.

Our results concur the report by Hwang et al. (2012) study, in which they also found the synergistic effect of Ag-NPs with AMI against *E. coli*. They also found the synergistic effect of Ag-NPs and KAN against all three test organisms. They proposed such results might be due to the differences in size of prepared Ag-NPs. Fayaz et al. (2010) also studied the combined antimicrobial effect of antibiotics and Ag-NPs and suggested that the increase in synergistic effect may be caused by the bonding reaction between antibiotic and Ag-NPs. Birla et al. (2009) also observed the enhanced synergistic antimicrobial effect of antibiotics like vancomycin, gentamycin, streptomycin, ampicillin, and kanamycin when applied in combination with Ag-NPs against *P. aeruginosa, S. aureus,* and *E. coli*. In literature, it is proposed that the antimicrobial action of Ag-NPs occurs through the alteration of cell membrane permeability, morphology, separation of the cytoplasmic membrane from the cell wall, plasmolysis, breakdown of DNA, and inhibition of respiratory activity (Jung et al. 2008; Li et al. 2011; Fayaz et al. 2010; Birla et al. 2009). From the results of present study, it is proposed that the Ag-NPs might be disrupting the bacterial cell wall structure and surface charge balance, which eventually change the permeability of bacterial cell wall due to which antibiotics have better opportunity to approach the individual bacterial cell associated with biofilm.

Antibiofilm potential of Ag-NPs

According to the report of the National Institutes of Health and Center of Disease control, about ~65–80 %

Table 2 The ΣFIC index range of Ag-NPs with four antibiotics against three test bacterial strains

	S. aureus		*E. coli*		*P. aeruginosa*	
	E. nidulans	*A. flavus*	*E. nidulans*	*A. flavus*	*E. nidulans*	*A. flavus*
AMI	0.188–1.5	0.5–0.625	0.094–0.75	0.078–0.625	0.312–1.5	0.31–1.25
KAN	0.14–1.125	0.094–0.375	0.078–2.5	0.14–1.25	ND	0.515–1.031
OXY	0.133–1.063	0.07–0.281	0.078–2.5	0.14–1.25	ND	0.265–1.063
STR	0.156–1.25	0.07–0.281	0.069–0.565	0.07–0.565	0.07–1.125	0.31–1.25

ND not detected

Table 3 The ΣFIC index mean of Ag-NPs with four antibiotics against three test bacterial strains

	S. aureus		*E. coli*		*P. aeruginosa*	
	E. nidulans	*A. flavus*	*E. nidulans*	*A. flavus*	*E. nidulans*	*A. flavus*
AMI	0.713^{PS}	0.563^{PS}	0.351^{S}	0.051^{S}	0.887^{PS}	0.859^{PS}
KAN	0.726^{PS}	0.258^{S}	0.716^{PS}	0.523^{PS}	ND^{A}	0.945^{PS}
OXY	0.55^{PS}	0.231^{S}	0.963^{PS}	0.712^{PS}	ND^{A}	0.841^{PS}
STR	0.509^{PS}	0.129^{S}	0.364^{S}	0.332^{S}	0.679^{PS}	0.687^{PS}

PS partial synergistic, *S* synergistic, *A* antagonism, *ND* not detected

infections occurred by biofilm formation microbes, amid which the Gram-negative bacterium *P. aeruginosa, E. coli*, and the Gram-positive *staphylococci, S. aureus* are the most common ones (Joo and Otto 2012). Ag-NPs have an exclusive ability to disrupt biofilm of several pathogenic bacteria. Biosynthesized Ag-NPs were tested for biofilm inhibition potential against *E. coli, P. aeruginosa*, and *S. aureus*, having known of their ability to form biofilm. Test organisms were grown in microtiter plate wells with and without Ag-NPs to form biofilm for 24 h. The treatment of cell-free filtrate (positive control) did not show any significant decrease in the biofilm formation. The fungal cell-free filtrate showed 4–6 % antibiofilm activity in the absence of Ag-NPs, while treatment with concentration of 0.5–64 µg/mL of both Ag-NPs resulted in a significant decrease of 74–84 % (Figs. 5, 6) in the biofilm formation. In the both cases, the amount of biofilm formation was sharply decreased by increase in Ag-NPs concentration. The AfAg-NPs (at 2 µg/mL) reduce the biofilm formation up to 70 % in both gram-negative bacteria, whereas with gram-positive bacteria, it produces 30 % reduction. While in case of EnAg-NPs, the ≥50 % inhibition in biofilm formation was seen at 4 µg/mL for *S. aureus* and *P. aeruginosa*, and 8 µg/mL for *E. coli*. The IC_{50} values for AfAg-NPs were 9.9, 1.817, and 3.207 µg/mL against *S. aureus*, *P. aeruginosa*, and *E. coli*, respectively, whereas in case of EnAg-NPs these are 18.06, 4.165, and 10.08 µg/mL, respectively. From the above data, it was seen that the AfAg-NPs were better antibiofilm agents against the gram-negative bacteria than the EnAg-NPs. This difference in the inhibitory activity of both Ag-NPs can also be explained by several factors, including efficacy in antimicrobial activity, physical properties like size of nanoparticles, which affect the limited penetration and other chemical properties like affinity between the materials and the biofilms (Park et al. 2013). Park et al. (2013) also proposed that the biosorption might be responsible for the biofilm inactivation in *P. aeruginosa*, and Ag-NPs inactivated *P. aeruginosa* biofilm cells in a biosorption-dependent manner. Kalishwaralal et al. (2010) also demonstrated that nanoparticles inhibited *P. aeruginosa* growth by ceasing the exopolysaccharide synthesis, consequently inhibiting biofilm formation. They found that 50 nM of Ag-NPs significantly arrested biofilm formation without affecting viability, whereas 100 nM inhibited the growth of the *P. aeruginosa* itself and led to 95 % reduction in biofilm. Goswami et al. (2015) also studied the Ag-NPs mediated biofilm eradication, and found inhibition of 89 % for *S. aureus* and 75 % for *E. coli* at 15 mg/mL. The data in the present study validate that Ag-NPs can effectively and rapidly detach biofilm, produced by *E. coli*, *P. aeruginosa,* and *S. aureus* at clinically achievable concentrations of silver nanoparticles. This implies, the application of these Ag-NPs as biofilm-disrupting agents.

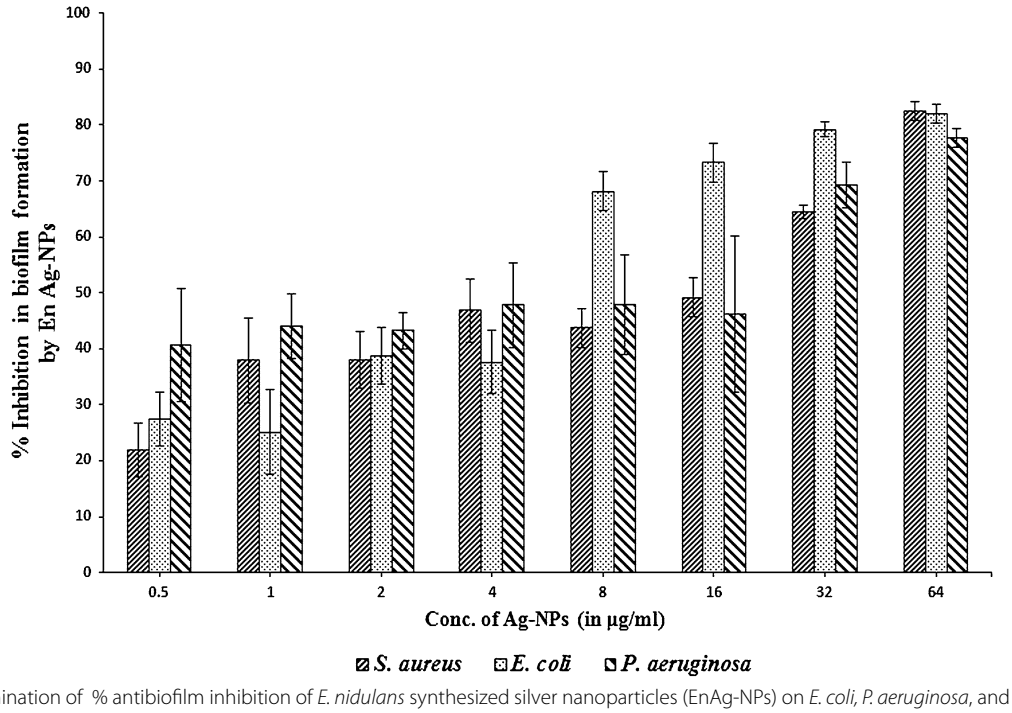

Fig. 5 Determination of % antibiofilm inhibition of *E. nidulans* synthesized silver nanoparticles (EnAg-NPs) on *E. coli, P. aeruginosa*, and *S. aureus* by microtiter plate method

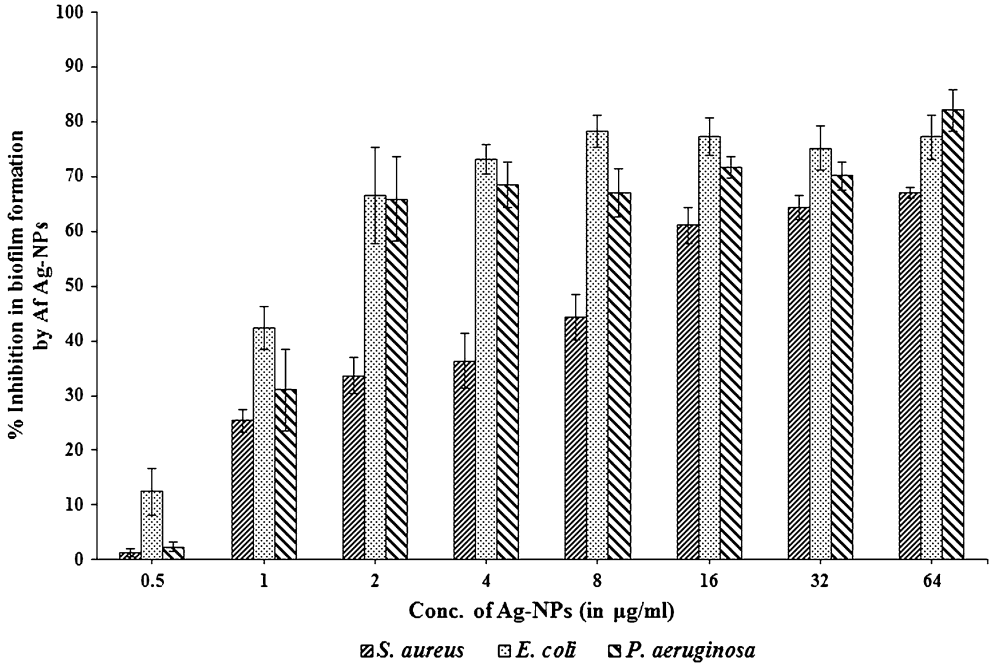

Fig. 6 Determination of % antibiofilm inhibition of *A. flavus* synthesized silver nanoparticles (AfAg-NPs) on *E. coli, P. aeruginosa,* and *S. aureus* by microtiter plate method

Conclusions

In the present study, the biosynthesis method used for synthesizing Ag-NPs has a distinct advantage over chemical synthetic techniques such as a high efficiency, biocompatibility, ecofriendly, and low toxicity to the environment. In this work, a new fungal source (*E. nidulans*) is reported as a potential source of Ag-NPs synthesis. As per the available knowledge, we are the first to report the formation of hexagonal-shaped Ag-NPs by the fungus as confirmed by TEM analysis. UV–visible absorbance spectral analysis confirmed the surface plasmon resonance of biosynthesized Ag-NPs. XRD, FTIR, and EDX provided additional strong evidence of biological synthesis of Ag-NPs and the crystallinity of the synthesized Ag-NPs. Furthermore, the biosynthesized Ag-NPs displayed a pronounced antimicrobial and antibiofilm potential against different clinically important pathogenic microorganisms. Since high CFU is applied in this study, it appears that these particles could have an excellent bactericidal effect and are effective in reducing bacterial growth for practical applications and the formulation of various biocidal materials. The synergistic action of antimicrobial agents can reduce the need for high dosages and minimize side effects. This study demonstrates the synergistic effect of antibiotics and nanoparticles in improving their bactericidal property; it was suggested that nanoparticles can be effectively used in combination with antibiotics in order to improve their efficacy against various pathogenic microbes.

Abbreviations

Ag-NPs: silver nanoparticles; AfAg-NPs: *Aspergillus flavus* synthesized silver nanoparticles; EnAg-NPs: *Emericella nidulans* synthesized silver nanoparticles; MBC: minimum bactericidal concentration; FICI: fractional inhibitory concentration index; FTIR: fourier transform infrared spectrometer; TEM: transmission electron microscopy; XRD: X-ray diffraction; EDX: Energy-dispersive X-ray spectroscopy.

Authors' contributions

AB was involved in the synthesis of Ag-NPs, antibiotic synergism study, antimicrobial and antibiofilm activity and the preparation of the manuscript. KRA helped in the synthesis and characterization of Ag-NPs. HJ was involved in the formulation of hypothesis and concept and design of the experiments. All the authors are involved in the drafting and revision of the manuscript. All the authors read and approved the final manuscript.

Acknowledgements

The authors gratefully acknowledge the University Grant Commission (UGC), New Delhi, India for financial support (vide nos. F.41-543/2012 (SR)). The authors also gratefully acknowledge SAIF (DST), Department of Anatomy, AIIMS, New Delhi, India for TEM analysis; Department of Pharmacy, Guru Ghasidas Vishwavidyalaya, Bilaspur, C.G., India for FTIR analysis; NIT Raipur for EDX analysis; and Sophisticated Analytical Instrumental Laboratory (SAIL), School of Pharmaceutical Sciences, Rajiv Gandhi Proudyogiki Viswavidyalaya, Bhopal, M.P., India for particle size analysis.

Competing interests

The authors declare that they have no competing interests.

Received: 7 September 2015 Accepted: 20 January 2016
Published online: 12 February 2016

References

Bhainsa KC, D'Souza SK (2006) Extracellular biosynthesis of silver nanoparticles using the fungus *Aspergillus fumigatus*. Colloids Surf B 47:160–164

Bihari P, Vippola M, Schultes S, Praetner M, Khandoga A, Reichel C, Coester C, Tuomi T, Rehberg M, Krombach F (2008) Optimized dispersion of nanoparticles for biological in vitro and in vivo studies. Part Fiber Toxicol 5:1–14

Birla SS, Tiwari VV, Gade AK, Ingle AP, Yadav AP, Rai MK (2009) Fabrication of silver nanoparticles by *Phoma glomerata* and its combined effect against *Escherichia coli*, *Pseudomonas aeruginosa* and *Staphylococcus aureus*. Lett Appl Microbiol 48:173–179

Botelho MG (2000) Fractional inhibitory concentration index of combinations of antibacterial agents against cariogenic organisms. J Dent 28:565–570

Chatterjee AK, Sarkar RK, Chattopadhyay AP, Aich P, Chakraborty R, Basu T (2012) A simple robust method for synthesis of metallic copper nanoparticles of high antibacterial potency against *E. coli*. Nanotechnology 23:085103

Chaturvedi V, Verma P (2015) Fabrication of silver nanoparticles from leaf extract of *Butea monosperma* (flame of forest) and their inhibitory effect on bloom-forming cyanobacteria. Bioresour Bioprocess 2:18

Chudasama B, Vala AK, Andhariya N, Mehta RV, Upadhyay RV (2010) Highly bacterial resistant silver nanoparticles: synthesis and antibacterial activities. J Nanopart Res 12:1677–1685

Durán N, Marcato PD, Durán M, Yadav A, Gade A, Rai M (2011) Mechanistic aspects in the biogenic synthesis of extracellular metal nanoparticles by peptides, bacteria, fungi, and plants. Appl Microbiol Biotechnol 90:1609–1624

Fayaz AM, Balaji K, Girilal M, Yadav R, Kalaichelvan PT, Venketesan R (2010) Biogenic synthesis of silver nanoparticles and their synergistic effect with antibiotics: a study against gram-positive and gram-negative bacteria. J Nanomed Nanotechnol 6:103–109

Fazay AM, Girilal M, Rahman M, Venkatesan R, Kalaichelvan PT (2011) Biosynthesis of silver and gold nanoparticle using thermophilic bacterium *Geobacillus stearothermophilus*. Process Biochem 46:1958–1962

Goswami SR, Sahareen T, Singh M, Kumar S (2015) Role of biogenic silver nanoparticles in disruption of cell-cell adhesion in *Staphylococcus aureus* and *Escherichia coli* biofilm. J Ind Eng Chem 26:73–80

Hwang I, Hwang JH, Choi H, Kim K, Lee DG (2012) Synergistic effects between silver nanoparticles and antibiotics and the mechanisms involved. J Med Microbiol 61:1719–1726

Ingle A, Rai M, Gade A, Bawaskar MJ (2009) *Fusarium solani*: a novel biological agent for the extracellular synthesis of silver nanoparticles. J Nanopart Res 11:2079–2085

Isenberg HD (2007) Synergism testing: broth microdilution checkerboard and broth macrodilution methods: In: Garcia LS (ed) Clinical microbiology procedures handbook, vol 2E. Microbiology ASM, p 5.12.1

Jaidev LR, Narasimha G (2010) Fungal mediated biosynthesis of silver nanoparticles, characterization and antimicrobial activity. Colloids Surf B 81:430–433

Jain N, Bhargava A, Majumdar S, Tarafdar JC, Panwar J (2011) Extracellular biosynthesis and characterization of silver nanoparticles using *Aspergillus flavus* NJP08: a mechanism perspective. Nanoscale 3:635–641

Joo HS, Otto M (2012) Molecular basis of in vivo biofilm formation by bacterial pathogens. Chem Biol 19:1503–1513

Jung WK, Koo HC, Kim KW, Shin S, Kim SH, Park YH (2008) Antibacterial activity and mechanism of action of the silver ion in *Staphylococcus aureus* and *Escherichia coli*. Appl Environ Microbiol 74:2171–2178

Kalishwaralal K, Kanth SBM, Pandian SRK, Deepak V, Gurunathan S (2010) Silver nanoparticles impede the biofilm formation by *Pseudomonas aeruginosa* and *Staphylococcus epidermidis*. Colloids Surf B 79:340–344

Keat CL, Aziz A, Eid AM, Elmarzugi NA (2015) Biosynthesis of nanoparticles and silver nanoparticles. Bioresour Bioprocess 2:47

Khatami M, Pourseyedi S, Khatami M, Hamidi H, Zaeifi M, Soltani L (2015) Synthesis of silver nanoparticles using seed exudates of *Sinapis arvensis* as a novel bioresource, and evaluation of their antifungal activity. Bioresour Bioprocess 2:19

Kim JS, Kuk E, Yu KN, Kim JH, Park SJ, Lee HJ, Kim SH, Park YK, Park YH, Hwang CY, Kim YK, Lee YS, Jeong DH, Cho MH (2007) Antimicrobial effects of silver nanoparticles. Nanomed Nanotechnol Bio Med 3:95–101

Kora AJ, Arunachalam J (2011) Assessment of antibacterial activity of silver nanoparticles on *Pseudomonas aeruginosa* and its mechanism of action. World J Microbiol Biotechnol 27:1209–1216

Li WR, Xie XB, Shi QS, Duan SS, Ouyang YS, Chen YB (2011) Antibacterial effect of silver nanoparticles on *Staphylococcus aureus*. Biometals 24:135–141

Li G, He D, Qian Y, Guan B, Gao S, Cui Y, Yokoyama K, Wang L (2012) Fungus-mediated green synthesis of silver nanoparticles using *Aspergillus terreus*. Int J Mol Sci 13:466–476

Marambio-Jones C, Hoek EMV (2010) A review of the antibacterial effects of silver nanomaterials and potential implications for human health and the environment. J Nanopart Res 12:1531–1551

McShan D, Ray PC, Yu H (2014) Molecular toxicity mechanism of nanosilver. J Food Drug Anal 22:116–127

Nath D, Banerjee P (2013) Green nanotechnology—a new hope for medical biology. Environ Toxicol Pharmacol 36:997–1014

Noguez C (2007) Surface plasmons on metal nanoparticles: the influence of shape and physical environment. J Phys Chem C 111:3806–3819

Pal S, Tak YK, Song JM (2007) Does the antibacterial activity of silver nanoparticles depend on the shape of the nanoparticle? a study of the gram-negative bacterium *Escherichia coli*. Appl Environ Microbiol 73:1712–1720

Park H, Park S, Roh J, Kim S, Choi K, Yi J, Kim Y, Yoon J (2013) Removal characteristics of engineered nanoparticles by activated sludge. J Ind Eng Chem 19:614–619

Pelletier DA, Suresh AK, Holton GA, McKeown CK, Wang W, Gu B, Mortensen NP, Allison DP, Joy DC, Allison MR, Brown SD, Phelps TJ, Doktycz MJ (2010) Effects of engineered cerium oxide nanoparticles on bacterial growth and viability. Appl Environ Microbiol 76:7981–7989

Quester K, Avalos-Borja M, Castro-Longoria E (2013) Biosynthesis and microscopic study of metallic nanoparticles. Micron 54–55:1–27

Ramaswamy RK, Krishnamurthy PP, Kaliannan T (2012) Mycogenic synthesis of silver nanoparticles by the Japanese environmental isolate *Aspergillus tamarii*. J Nanopart Res 14:860–862

Roy N, Gaur A, Jain A, Bhattacharya S, Rani V (2013) Green synthesis of silver nanoparticles: an approach to overcome toxicity. Environ Toxicol Pharmacol 36:807–812

Saravanan M, Nanda A (2010) Extracellular synthesis of silver bionanoparticles from *Aspergillus clavatus* and its antimicrobial activity against MRSA and MRSE. Colloids Surf B 77:214–218

Sintubin L, Verstraete W, Boon N (2012) Biologically produced nanosilver: current state and future perspectives. Biotechnol Bioeng 109:2422–2436

Thirunavoukkarasu M, Balaji U, Behera S, Panda PK, Mishra BK (2013) Biosynthesis of silver nanoparticle from leaf extract of *Desmodium gangeticum* (L.) DC. and its biomedical potential. Spectrochim Acta Part A 116:424–427

Vigneshwaran N, Ashtaputre NM, Varadarajan PV, Nachane RP, Paralikar KM, Balasubramanya RH (2007) Biological synthesis of silver nanoparticles using the fungus *Aspergillus flavus*. Mater Lett 61:1413–1418

Yoon K, Byeon JH, Park J, Hwang J (2007) Susceptibility constants of *Escherichia coli* and *Bacillus subtilis* to silver and copper nanoparticles. Sci Total Environ 373:572–575

Zhao K, Zhao J, Wu C, Zhang S, Deng Z, Hu X, Chen M, Peng B (2015) Fabrication of silver-decorated sulfonated polystyrene microspheres for surface-enhanced Raman scattering and antibacterial applications. RSC Adv 5:69543–69554